J. Fluid Mech. (2005), *vol.* 539, *pp.* 1–24.
doi:10.1017/S0022112004002666 Printed in the United Kingdom

Shallow flow past a cylinder: control of the near wake

By H. FU AND D. ROCKWELL

Lehigh University, Department of Mechanical Engineering and Mechanics, 354 Packard Laboratory, 19 Memorial Drive West, Bethlehem, PA 18015, USA
dor0@lehigh.edu

(Received 23 February 2004 and in revised form 27 September 2004)

Vortex formation in the near wake of shallow flow past a vertical cylinder can be substantially delayed by base bleed through a very narrow slot. The structure of the wake associated with this delay changes dramatically with the dimensionless momentum coefficient of the slot bleed. At very low values, where substantial vortex delay is attainable, the bleed flow is barely detectable. For progressively larger values, various forms of jets issue from the slot, and they undergo ordered, large-amplitude undulations, not necessarily synchronized with the formation of the large-scale vortices. When the cylinder is subjected to appropriate rotational perturbations, in the presence of small-magnitude base bleed, it is possible to transform the delayed vortex formation to a form characteristic of the naturally occurring vortices and, furthermore, to induce a large change of the phase, or timing, of the initially formed vortex, relative to the cylinder motion.

These features of the near-wake structure are assessed via a technique of high-image-density particle image velocimetry, which provides whole-field patterns of vorticity, Reynolds stress, amplitude distributions of spectral peaks, and streamline topology at and above the bed, for both the delayed and recovered states of the wake. Among the findings is that even small bleed can substantially alter the patterns of streamline topology and Reynolds stress at the bed, which has important consequences for the bed loading.

These alterations of the near-wake structure occur in conjunction with modifications of the shallow approach flow, which is incident upon the upstream face of the cylinder. The topology at the bed, which is altered in accord with attenuation of the well-defined vorticity concentration of the horseshoe (standoff) vortex, shows distinctive patterns involving new arrangements of critical points.

1. Introduction

1.1. *Previously related investigations*

During the past two decades, a range of investigations have clearly established the existence of a large-scale Kármán-like instability in the near wake of a cylinder or bluff body in a shallow flow, whereby the characteristic diameter or width of the body is larger than the depth of the flow. Particularly striking is the occurrence of these instabilities in oceanographic and atmospheric flows, involving flow past an island or a mountain. Representative, recent works include those of Ingram & Chu (1987) and Smith & Grubisic (1993), as well as the investigations cited therein.

In the laboratory setting, the essential features of the near-wake instability, as well as its attenuation due to bed friction effects, have been investigated by Ingram & Chu (1987), Chen & Jirka (1995), Carmer, Weitbrecht & Jirka (2001), Carmer, Rummel & Jirka (2002, 2003), Akilli & Rockwell (2002) and Kahraman, Sahin & Rockwell (2002). All of these investigations have focused on the geometry of a right circular cylinder. Equivalent, large-scale instabilities in the near wake can be generated behind a flat plate normal to the free stream, as shown by Chen & Jirka (1995), Balachandar, Tachie & Chu (1999), Balachandar, Ramachandran & Tachie (2000) and Tachie & Balachandar (2001). Furthermore, nominally cylindrical configurations, with finite side slope to simulate actual islands, can also lead to the generation of large-scale instabilities, as demonstrated by Lloyd & Stansby (1997) for the case of steady inflow and Lloyd, Stansby & Chen (2001) for the case of oscillatory flow.

An important dimensionless parameter which, in effect, accounts for the simultaneous influence of destabilization in the near wake due to transverse shear flow, and stabilization arising from bed friction effects, is the stability parameter $S = c_f D/h_w$, in which c_f is the quadratic friction coefficient, D is the cylinder diameter and h_w is the depth of the shallow water layer. Details on the origin of this type of instability parameter are provided by Ingram & Chu (1987). As demonstrated by Chen & Jirka (1997), it can effectively aid the interpretation of computed global (absolute) and convective instabilities of the near wake. From a physical standpoint, a number of unstable and stable wake modes can occur, as characterized by Chen & Jirka (1995) and further assessed by Chen & Jirka (1997); the stability parameter S is central to defining the boundaries between these modes. Further insight into the unstable mode(s) of the near wake is provided by the earlier instability analyses and computations of Schar & Smith (1993) and Grubisic, Smith & Schar (1995). All of the foregoing analyses account for the possibility of a global (absolute) instability of the near wake, which leads to the nonlinear, highly robust limit-cycle oscillations associated with large-scale Kármán-like vortex formation in the near wake. These theoretical approaches are conceptually equivalent, in the absence of bed friction effects, to the well-known instability and vortex formation in the near wake of a cylinder of large spanwise extent, which is critically assessed by Huerre & Monkewitz (1990).

Control of the shallow near wake has received relatively little attention. Kahraman, *et al.* (2002) have demonstrated that a strip of surface elements of small height located on the bed at an appropriate location in the near wake region can lead to substantial attenuation, or retardation, of the process of large-scale vortex formation. Another approach involves the generation of a shallow wake from a porous bluff body, i.e. a porous plate, as described by Chen & Jirka (1995). They employed dye visualization to classify the patterns of the near-wake structure while accounting for the magnitude of the reverse velocity along the central portion of the wake. In turn, these features were interpreted in the context of the aforementioned wake stability parameter $S = c_f D/h_w$. In essence, Chen & Jirka (1995) demonstrated that it is possible to completely attenuate the mechanism of absolute (global) instability leading to large-scale vortex formation in the shallow wake. This result is in accord with the investigation of a wake of very large spanwise extent past a porous plate, investigated by Inoue (1985). These findings build upon the earlier investigation of Castro (1971), who demonstrated attenuation of the near-wake vortex formation via base bleed from porous plates of large spanwise extent. Base bleed has also been shown to substantially alter the formation process of vortices from a streamlined body with a blunt trailing edge, as demonstrated by Wood (1964, 1967) and Bearman (1967).

Another approach, which is equivalent to the aforementioned concept of base bleed, is self-bleed through a slit cut along the entire span of the cylinder, as described by Igarashi (1978), who demonstrated that the region of vortex formation was displaced significantly downstream, relative to the case of a plain cylinder. Wong (1985) pursued a more advanced approach involving self-injection at two locations near the base of the cylinder, whereby the injection flow was through an annulus opened at the forward stagnation point. This technique was applied to an elastically mounted cylinder, and it was demonstrated that vibrations could be suppressed completely when the effective injection rate was very small. In all of these investigations involving base bleed, with some exceptions, relatively little information is available on the quantitative flow structure associated with the concept of base bleed.

Irrespective of the type of bluff body that generates the unstable or stable mode of the near wake, a horseshoe (necklace) vortex system is formed about the upstream surface of the body. In recent years, a range of investigations have provided insight into the complex structure of the horseshoe vortex system in deep flows, i.e. flows in which the distance from the bed to a free surface or a bounding wall of a wind or water tunnel is large. Simpson (2001) provides a review of this class of junction flows. For the case of high Reynolds number, whereby the inflow boundary layer is turbulent, Devenport & Simpson (1990) characterized in detail the turbulence characteristics in the context of flow separation at a wing–body junction. For the case of lower Reynolds number (laminar) inflow, Visbal (1991) numerically calculated basic classes of horseshoe or necklace vortex patterns and the onset of a self-sustaining instability. More recently, Seal, Smith & Rockwell (1997), Praisner *et al.* (1997), Seal & Smith (1999) and Praisner, Sabatino & Smith (2001) investigated various aspects of the unsteady structure of the horseshoe (necklace) vortex system at the junction of a rectangular bluff body with a plate and a wing–plate junction. For the case where the height of the body is finite and small, Lawless, Lane & Best (2003) characterized in detail the junction vortex system for the configurations of a surface-mounted cylinder and cuboid. They describe the unsteadiness of the junction vortex system in terms of instantaneous patterns of the flow structure.

1.2. *Unresolved issues*

On the basis of previous investigations, it is clear that base bleed is an effective means of attenuating the process of vortex formation in the near wake of a bluff body and, furthermore, if the body is elastically mounted, the amplitude of vibration can be completely suppressed. A detailed knowledge of the flow physics is, however, lacking for the case of a cylinder of large spanwise extent, and our understanding is even more limited for the case of a shallow bluff-body wake, where the influence of the bed region becomes prevalent. More specifically, the major unclarified issues are as follows:

1. In an overall sense, the regimes of the near-wake response to varying magnitudes of slot bleed from the base have not been established for shallow flows. Such regimes are expected to include, first of all, at very low values of bleed flow, alteration of the near-wake vortex formation due to relief of the negative base pressure. Then for higher values of bleed, formation of a jet-like flow is expected; its relation to attenuation of the large-scale Kármán vortex formation is unclear.

2. Characterization of the effects of base bleed in terms of patterns of instantaneous and averaged vorticity, along with wholefield representations of spectra of the near-wake oscillation, including the distinction between the spectral content in the base region, relative to spectra at locations further downstream of the wake, has not been pursued.

3. The consequence of base bleed for the patterns of streamline topology and Reynolds stress correlation immediately adjacent to the bed, as well as at elevations above the bed, has not been addressed. Even for relatively small magnitudes of base bleed, it is anticipated that ordered patterns of low-velocity regions, as well as critical points, such as foci and saddle points, may be substantially altered relative to the case of no base bleed. In turn, these topological features are expected to be linked to the location and magnitude of extrema of Reynolds stress correlations.

4. In cases where attenuation, or retardation, of the large-scale vortex formation is attained via proper application of base bleed, the issue arises as to whether controlled, rotational perturbations of the cylinder can lead to recovery of large-scale vortex formation. In particular, it is of interest to establish the extent to which combined base bleed and rotational perturbations lead to recovery of the streamline topology and patterns of Reynolds stress associated with vortex formation from the corresponding plain cylinder.

5. All of the foregoing issues address alteration of the near-wake structure due to base bleed. In the event that the bleed flow is due to extraction of flow at the forward stagnation point, e.g. via a thin slot extending through the cylinder, then an important byproduct is possible alteration of the topological and vorticity patterns at and above the bed of the shallow inflow. In particular, there may be redistribution of the location and number of critical points adjacent to the bed, which represent the footprint of the horseshoe (necklace) vortex above the bed bounded by the free surface. In addition, alterations of the degree of concentration of vorticity of the horseshoe vortex may occur. These features have remained unexplored.

The overall goal of the present investigation is to address these issues using a technique of high-image-density particle image velocimetry, in a cinema mode, such that not only instantaneous, phase- and time-averaged representations are attainable, but also representations of spectra of the unsteadiness at a large number of grid points throughout the flow field.

2. Experimental system and techniques

Experiments were undertaken in a large-scale free-surface water channel. The flow from a large reservoir passes through a system of honeycomb-screen flow conditioning, then a 3:1 contraction, and finally to the main test section, which had a total length of 4318 mm, a width of 610 mm and a depth of 610 mm.

As indicated on figure 1(*a*), a long plate with an elliptical leading edge was employed to generate a shallow free-surface layer of desired thickness and inflow velocity. This plate had a width of 610 mm, a length of 3660 mm, and was at an elevation of 254 mm above the floor of the main test section. Furthermore, as shown in the schematic, an adjustable inclined plate allowed fine tuning of the volume flow along the upper and lower surfaces of the plate, and thereby the location of the stagnation point at the elliptical leading edge. A cylinder of diameter $D = 101.6$ mm was located a distance of 3048 mm from the leading edge of the plate. The vertical cylinder was made of transparent Plexiglas. As shown in figure 1, this cylinder could be subjected to controlled motion via a computer-controlled rotational system. The present experiments examine the effect of passive base bleed through a slot of width G. The cylinder shown in figure 1 had slot widths $G = 0$, designated as the plain cylinder, and $G = 1/64, 1/32, 1/16$, and $1/8$ in., corresponding to 1.58, 3.18, 6.35, and 12.70 mm. When normalized by the cylinder diameter $D = 4$ in. (101.6 mm), the values of $G/D = 0.016, 0.031, 0.062$ and 0.125. For these values of G/D, jet velocity

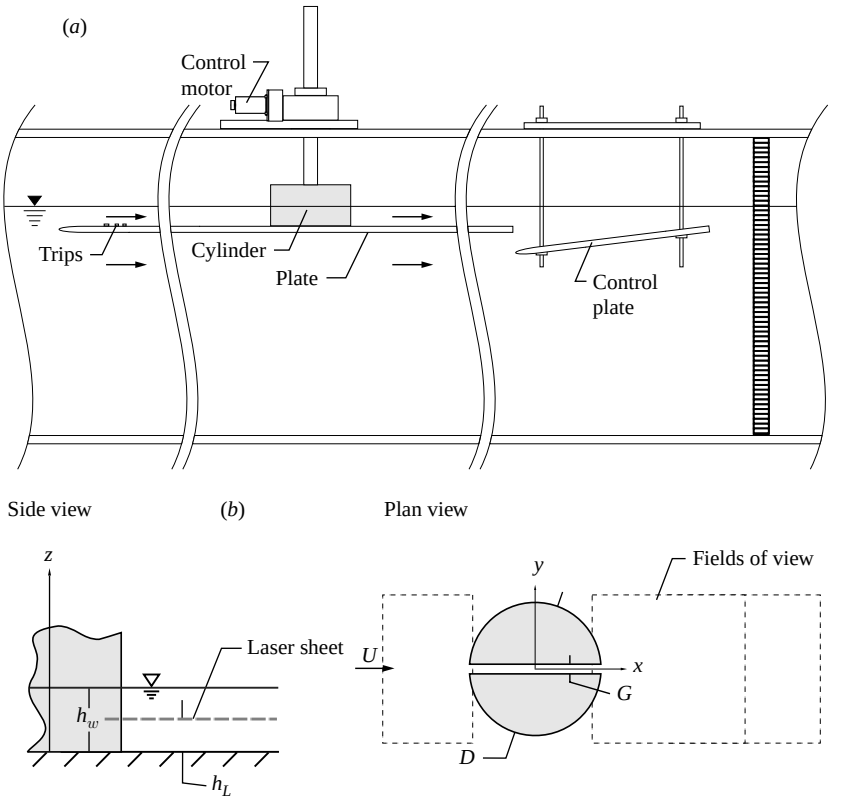

FIGURE 1. (*a*) Overall view of test section and (*b*) close-up plan and side views of the cylinder–plate arrangement.

V_j normalized by the depth-averaged inflow velocity U is $V_j/U = 0.66, 0.87$ and 1.0 respectively for $G/D = 0.031, 0.062$ and 0.125. Jet velocity V_j is averaged spatially over the cross-section of the slot at a location 5 mm upstream of the slot exit; moreover it is time-averaged as well in order to account for temporal fluctuations of the order of a few per cent. The corresponding values of momentum coefficient are $c_\mu = V_j^2 G/(U^2 D) = 0.014, 0.048$ and 0.130.

Design of the experiment required that the turbulent shallow inflow attain a fully evolved state immediately prior to its interaction with the cylinder. Kirkgöz & Ardiclioglu (1997) and Kahraman *et al.* (2002) have assessed the criteria for attainment of a fully developed state of such a free-surface layer. For the present experiment, the layer was maintained at a depth of $h_w = 25.4$ mm and the depth-averaged velocity was $U = 177.8\,\mathrm{mm\,s^{-1}}$, which gives a corresponding value of Reynolds number of $Re_h = 4498$. The approach length L from the leading edge of the plate to the location of the cylinder was $L/h_w = 120$. Independent measurements of Kahraman *et al.* (2002) indicated that the turbulent layer was fully evolved at this location. For the aforementioned value of depth-averaged velocity U, the corresponding Reynolds number, based on diameter D of the cylinder, was $Re_D = 18\,000$. Furthermore, the dimensionless stability parameter of the near wake was $S = c_f D/h_w = 0.026$. As shown by Chen & Jirka (1995), this value falls in the range of $S \leqslant 0.2$, for which self-excited formation of large-scale vortices is expected to occur in the near wake. In this equation for S, the value of c_f is defined according

to $c_f = f/4$, in which f is the Darcy–Weisbach friction factor, estimated from the smooth wall limit of the Moody friction diagram.

A technique of high-image-density particle image velocimetry was used to characterize the instantaneous and averaged flow structures in the approach and near-wake regions of the cylinder. The flow was seeded with 14.6 micron metallic-coated hollow plastic spheres. These particles were illuminated by a laser sheet generated from a dual pulsed Nd:Yag laser system. The thickness of the sheet was approximately 1.25 mm; it was generated via a combination of spherical and cylindrical lenses. As shown in figure 1, the laser sheet was positioned parallel to the bed (bottom surface of the plate) at the heights $h_L/h_w = 0.04$, 0.5 and 0.95, corresponding to elevations immediately adjacent to the bed, at the midplane and at the free surface. In order to determine the distributions of velocity within the slot, the laser sheet was oriented vertically, such that it was coincident with the plane of the symmetry of the slot; the viewing axis of the camera, which is located exterior to the test section, was orthogonal to this laser sheet.

Images were acquired using a CCD camera having a resolution of 1008×1018 pixels at a rate of thirty frames per second. The magnification factor was $M = 1{:}13.7$, which yielded fields of view of 125 mm $\times$ 126 mm. For each experimental run, 138 image pairs were obtained, with a 1 to 2 ms delay between each image pair. A total of five experimental runs were considered, and the averaged quantities were obtained by ensemble-averaging the computed quantities. Velocity vectors were evaluated via a cross-correlation technique, whereby patterns of particles in successive frames were correlated using a 32×32 pixel interrogation window with a 50% overlap. The effective grid size in the plane of the laser sheet was 2 mm $\times$ 2 mm. Using this approach, approximately 3782 velocity vectors were generated. The raw data obtained from the interrogation process were subjected to a low-pass filter having a cutoff frequency seven times the dominant vortex shedding frequency.

Furthermore, the velocity vector field was subjected to Gaussian smoothing, using a kernel value of 1.3. These velocity fields were then used to calculate instantaneous patterns of vorticity and streamline topology. Corresponding time-averaged patterns of vorticity $\langle\omega\rangle$ and streamline $\langle s\rangle$ topology were calculated from the time-averaged velocity field $\langle \boldsymbol{V}\rangle$. In addition, phase-averaged patterns of velocity $\langle \boldsymbol{V}\rangle_p$, vorticity $\langle\omega\rangle_p$ and streamline $\langle s\rangle_p$ topology were calculated using attainment of the maximum scale of the large-scale vorticity concentration in the near wake as a phase reference. The sectional streamlines were obtained by integrating, via a predictor–corrector method, the velocity vector fields in the plane defined by the laser sheet. Perry & Steiner (1987), among others, also determined streamline patterns in the three-dimensional flow of a nominally two-dimensional bluff-body wake of large spanwise extent, and refer to such streamlines as integrated streamlines, in order to distinguish them from patterns based on the assumption of two-dimensional flow. In such planar representations, the existence of a spiral-like streamline pattern with a focus at its centre indicates that the flow is three-dimensional and, furthermore, inward and outward spiralling streamline patterns correspond respectively to stable and unstable foci. A stable focus corresponds to local stretching along the axis of the nominally two-dimensional vortical structure, and an unstable focus corresponds to local compression. Visbal & Gordnier (1994) critically addressed these concepts via a numerical simulation for a three-dimensional vortex flow. Furthermore, for the case of an inherently three-dimensional turbulent boundary layer, Zhong, Huang & Adrian (1998) successfully employed planar measurements to identify critical points over a given cross-section of the flow. Furthermore, since images were acquired at a sufficiently high rate of

15 Hz, relative to the frequency f_o of large-scale vortex formation in the near wake, which had values in the range $0.38 \leqslant f_o \leqslant 0.57$ Hz, it was possible to determine the time-dependent variation of either the streamwise $u(t)$ or transverse $v(t)$ velocity at a given location in the flow. The spectral analysis was then carried out using the standard definition and procedure for calculation of the auto-spectral density given by Newland (1993, p. 120). In fact, this procedure could be applied to all grid point locations at which the velocity vector field was calculated, thereby yielding time histories at a large number of locations over the plane of the flow field. Then, either auto-spectral analysis at a given point, or cross-spectral analysis between two given points, could be carried out at each grid location(s), followed by construction of contours of constant spectral amplitude $|S(f)|$ and phase $|\phi(f)|$ over the entire plane of the flow field.

3. Alteration of approach flow patterns due to localized flow extraction

Although the primary emphasis of this investigation is modification of the near-wake structure due to bleed through a slot, an important byproduct is alteration of the approach flow along the upstream face of the cylinder.

Figure 2 shows the averaged streamline topology at the midplane, $h_L/h_w = 0.5$, and at the bed, $h_L/h_w = 0.04$, for values of dimensionless gap width G/D from 0.016 to 0.125. For values up to, and including, $G = 0.031$, the form of the topology is generally similar. At the bed, a well-defined saddle point occurs upstream of the cylinder surface. The region between the circumferential streamlines emanating from the saddle point and the surface of the cylinder involves upstream-oriented streamlines, which are associated with the horseshoe vortex in that region. This horseshoe vortex is apparently confined to a region significantly below the midplane. That is, all streamline patterns at the midplane show a pattern characteristic of a stagnation flow except at $G = 0.031$ where the effect of significant flow extraction into the slot is apparent.

For the larger values of $G/D = 0.062$ and 0.125, substantial alteration of the topology $\langle \Psi \rangle$ at the bed is evident. At $G/D = 0.062$, an additional saddle point occurs along the plane of symmetry in the vicinity of the slot entrance. At $G/D = 0.125$, the near-bed topology has undergone a fundamental transformation. Saddle points are no longer evident along the plane of symmetry. Rather, they appear at nearly mirror image locations.

Figure 3 shows a comparison of time-averaged velocity $\langle \boldsymbol{V} \rangle$, streamline topology $\langle s \rangle$ and vorticity $\langle \omega \rangle$ for the larger values of gap G/D. Consider the patterns of average velocity $\langle \boldsymbol{V} \rangle$ and streamline topology $\langle s \rangle$ shown in the first and second columns. Irrespective of the type of topology, it is evident that, in the vicinity of the saddle points, the magnitude of the velocity is small. Furthermore, in the vicinity of the cylinder, the magnitude of the near-bed velocity, which is oriented in a direction upstream from the cylinder, has a substantial magnitude.

The third column of figure 3 shows the patterns of averaged velocity $\langle \boldsymbol{V} \rangle$ and vorticity $\langle \omega \rangle$ on the vertical plane of symmetry, in the entrance region of the slot. For the smallest value of $G/D = 0.031$, a well-defined horseshoe (standoff) vortex is evident; it involves a single, well-defined concentration of vorticity. This pattern is very similar to that characterized in the investigations of Devenport & Simpson (1990) and Praisner *et al.* (2001) for the vortex system at the junction of a plate and a bluff body with no slot. At a larger gap $G/D = 0.062$, the concentration of vorticity is no longer evident, but a well-defined layer of lower-level vorticity is present. At the largest

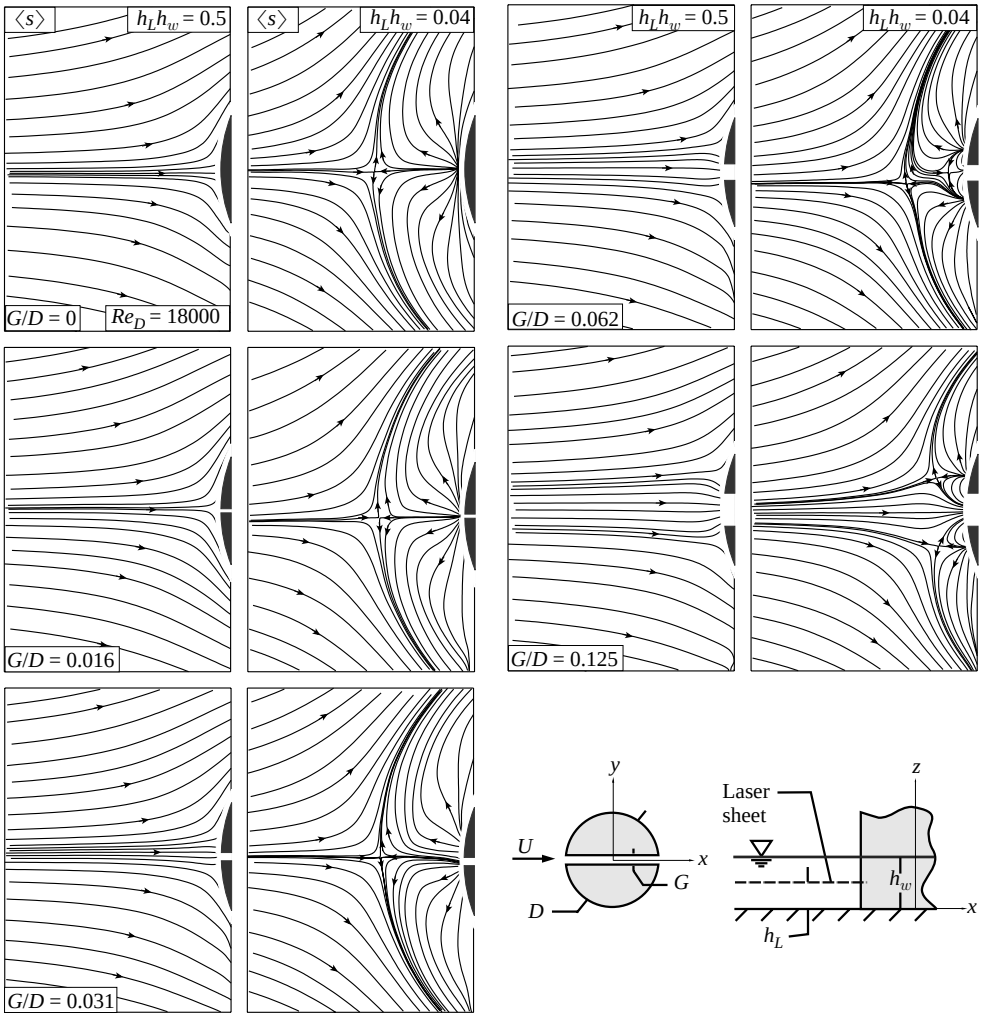

FIGURE 2. Time-averaged streamline topology of approach flow at the midplane $h_L/h_w = 0.5$ and immediately adjacent to the bed $h_L/h_w = 0.04$ for various values of dimensionless gap width G/D.

value $G/D = 0.125$, the gradient of this vorticity layer, in the direction normal to the wall, has further decreased. An additional observation from the images of vorticity $\langle\omega\rangle$ in the entrance region is the occurrence of vorticity concentrations at the junction between the free surface and the slot entrance. The generation of these concentrations is associated with small-amplitude, localized depressions of the free surface (not shown) in that region. The magnitude of the peak vorticity associated with these concentrations increases with increasing values of G/D. Irrespective of the existence of all the aforementioned vorticity concentrations, the velocity distribution within the slot rapidly smooths out, as shown in the shaded entrance region of each image.

Regarding the exit region of the slot, shown in the fourth column of images of figure 3, patterns of velocity vectors and vorticity show the transformation from the slot flow to the free jet. A significant vorticity layer exists along the bed for all values of G/D and the peak vorticity level decreases immediately upstream of the slot for successively larger values of dimensionless gap width G/D. For all values of G/D, the

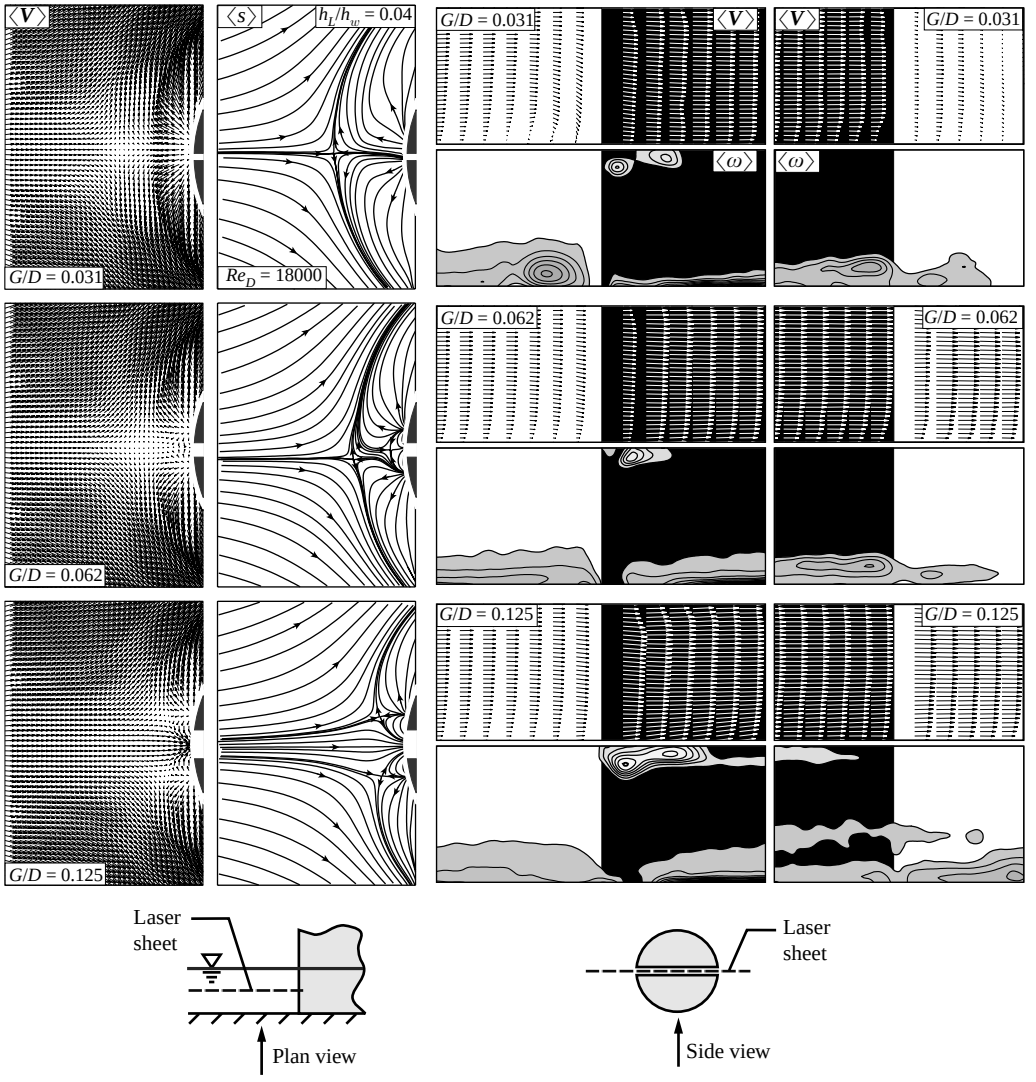

FIGURE 3. Comparison of time-averaged velocity $\langle \boldsymbol{V} \rangle$, streamline topology $\langle s \rangle$, and vorticity $\langle \omega \rangle$ in plan and side views, for variations of dimensionless gap width G/D.

velocity distribution is nearly uniform along its vertical extent, except in the region adjacent to the bed surface, in accord with the aforementioned vorticity layer. It is notable that, for the case of slot width $G/D = 0.031$, there exists a vertical stagnation line across the water layer, which is indicated by the very low magnitudes of velocity vectors in the rightmost profile. As will be shown subsequently in plan views of the flow topology, this interpretation is consistent with the occurrence of a saddle point at this location on the plane of symmetry of the cylinder wake, at elevations adjacent to and above the bed.

4. Near-wake vortex formation in the presence of slot bleed

Patterns of instantaneous velocity $\boldsymbol{V}$, streamline topology s, and vorticity ω are given in figure 4 as a function of gap width G/D. All patterns are phase-referenced

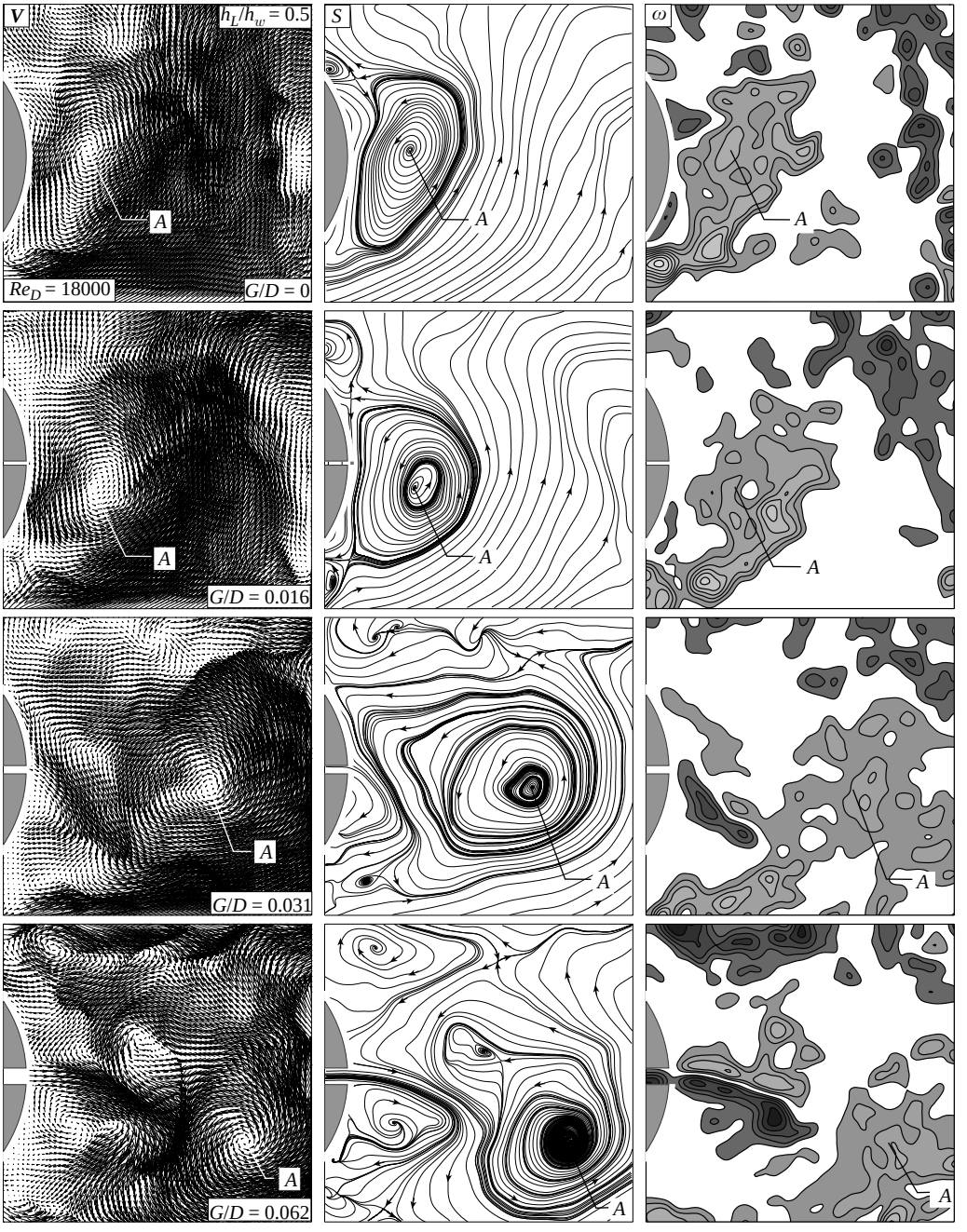

FIGURE 4. Patterns of instantaneous velocity $\boldsymbol{V}$, streamline topology s, and vorticity ω as a function of gap width G/D. All patterns are phase-referenced according to completion of formation of the large-scale vortex from the bottom surface of the cylinder. Images are on the midplane, $h_L/h_w = 0.5$, between the bed and the free surface.

according to the same phase of the cycle of vortex formation. This phase corresponds to attainment of the fully formed large-scale vortex from the bottom surface of the cylinder. At $G/D = 0$, the patterns of ω, $\boldsymbol{V}$, and s indicate that vortex formation occurs immediately adjacent to the base (downstream surface) of the cylinder. The

focus (apparent centre) of the pattern of streamline topology is designated as A, which, of course, corresponds to the centre of the spiral pattern of $\boldsymbol{V}$ shown in the left column, and the centre of the vorticity concentration in the right column. The same designation A is employed for larger values of G/D.

For the gap width $G/D = 0.016$, the focus of the s pattern, as well as the $\boldsymbol{V}$ pattern is displaced slightly downstream of those at $G/D = 0$. Correspondingly, a discernible downstream shift of the ω cluster is also evident. At $G/D = 0.031$, the large-scale vortex is displaced substantially downstream and, furthermore, layers of elongated positive and negative vorticity are evident in the vicinity of the slot; they are due to the jet flow from the slot exit. All of these effects become even more pronounced at $G/D = 0.062$, where the jet from the slot is more clearly defined, as evident in the patterns of $\boldsymbol{V}$, s and ω.

Figure 5 shows the time history of the jet development for $G/D = 0.125$. The patterns of velocity in the left column of images show a low-frequency, transverse undulation. The sequence of images extends over one half-cycle of the oscillation. As is evident from the values of the frame number N, which extend up to $N = 72$, corresponding to the end of the half-cycle, the period of this transverse oscillation is relatively large. In fact, it exceeds the period of the inherent large-scale vortex formation, in the absence of the slot, by a factor of approximately seven. Corresponding patterns of instantaneous vorticity ω are given in the right column of figure 5. Over the right half of the image $N = 1$, the positive and negative vorticity layers diverge substantially and, tend to interact with the clusters of vorticity of the separating layers from the bottom and top surfaces of the cylinder. For subsequent values of N, the transverse undulation of the jet results in different degrees of proximity, i.e. interaction, between a vorticity layer of the jet and a vorticity layer from the surface of the cylinder.

5. Inter-relationship between patterns of Reynolds stress correlation, spectral amplitudes, and streamline topology

Figure 6 shows patterns of time-averaged vorticity contours $\langle\omega\rangle$ in comparison with contours of constant amplitude of the spectral peak $|S_v(f, x, y)|$ of the near-wake velocity fluctuation v in the transverse direction.

Patterns of $\langle\omega\rangle$ are shown in the left column of images. At $G/D = 0$, large-scale clusters exist close to the base of the cylinder. At $G/D = 0.016$, they are significantly displaced in the downstream direction. At $G/D = 0.031$, the downstream displacement is very substantial indeed, and, for even larger values of $G/D = 0.062$ and 0.125, they transform to two nearly parallel, separating layers, with only mild deflections towards the wake centreline. This transformation of the large-scale clusters of $\langle\omega\rangle$ is accompanied by the onset of small-scale clusters of $\langle\omega\rangle$ in the vicinity of the slot exit at $G/D = 0.031$, which is associated with a jet undergoing large-amplitude transverse undulations. At larger values of $G/D = 0.062$ and 0.125, the spatial extent and peak amplitudes of these jet clusters of $\langle\omega\rangle$ become more prevalent. Moreover, the overall form of these clusters is altered. They are indicative of smaller-amplitude transverse undulations, relative to the flipping of the jet between the upper and lower surfaces of the cylinder at the lower value of slot width $G/D = 0.031$.

Also shown in the left column of images of figure 6 are spectra of the transverse velocity fluctuation v evaluated at two representative locations a and b in the near-wake region. Location a is immediately downstream of the slot exit and represents the transverse undulation of the jet. On the other hand, b is in the region where

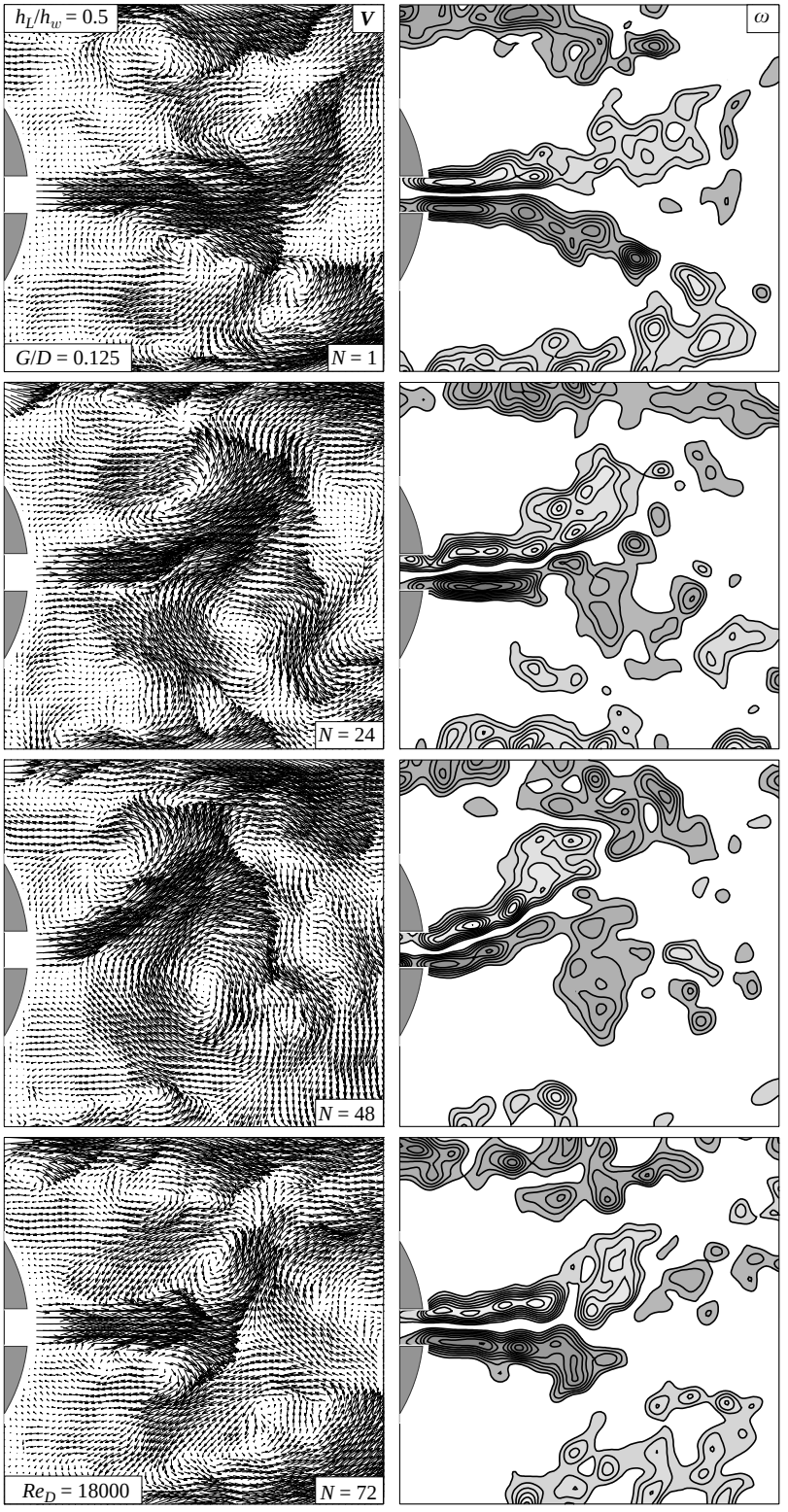

FIGURE 5. Time history of jet development for slot width $G/D = 0.125$. The sequence of patterns of instantaneous velocity $\boldsymbol{V}$ and vorticity ω are on the midplane, $h_L/h_w = 0.5$, and extend over one half-cycle of the jet oscillation.

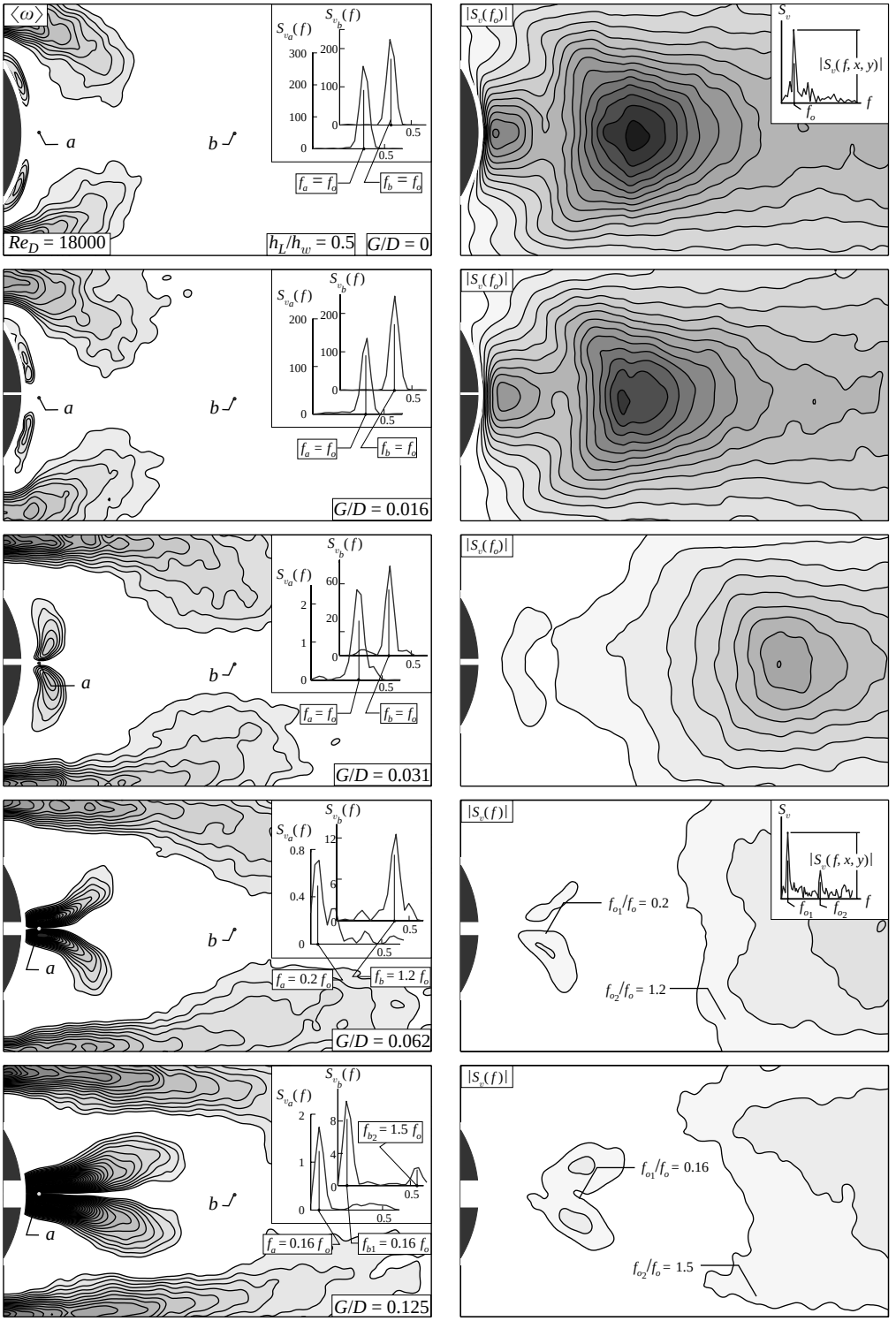

FIGURE 6. Patterns of time-averaged contours of vorticity $\langle\omega\rangle$ in comparison with contours of the spectral peak $|S_v(f)|$ of the transverse velocity component. Minimum and incremental values of spectral amplitude are $[|S_v(f_o)|]_{\min} = 5$ and $\Delta|S_v(f_o)| = 5$, except for $[|S_v(f_{o1})|]_{\min} = 4$ and $\Delta|S_v(f_{o1})| = 2$. Minimum and incremental levels of vorticity are $\langle\omega\rangle_{\min} = \pm 3\,\mathrm{s}^{-1}$ and $\Delta\langle\omega\rangle = 1\,\mathrm{s}^{-1}$.

large-scale vortices are formed. The spectra given in the inset of each image show, first of all, for values of $G/D = 0$, 0.016 and 0.031, the same predominant spectral component at locations a and b, i.e. $f_a = f_b = f_o$, in which $f_o \approx 0.38$ Hz is the frequency of formation of the large-scale vortical structures from the plain ($G/D = 0$) cylinder. It should be noted, however, that the peak spectral amplitudes at $G/D = 0.031$ are substantially attenuated relative to those at $G/D = 0$ and 0.016. When the gap width becomes sufficiently large, $G/D = 0.062$, the region near the slot exit is dominated by an undulating jet having a spectral peak at a low value of $f_a = 0.2 f_o$, while the spectral peak at the downstream location b indicates a slightly elevated formation frequency $f_b = 1.2 f_o$ of the large-scale vortices. At the largest value of $G/D = 0.125$, the low-frequency undulation occurs over a much more extensive region downstream of the slot exit, with a spectral peak at $f_a = 0.16 f_o$, while at the downstream location b, two spectral peaks are detectable: a dominant peak at $f_{b1} = 0.16 f_o$; and a smaller peak at $f_{b2} = 1.5 f_o$.

The spectral peaks shown in the left column of figure 6 are representative of those that were determined at a total of 5684 points throughout the flow field. Considering these spectral amplitudes, it is possible to construct contours of constant amplitude $|S_v(f, x, y)|$ throughout the flow domain, as indicated in the right column of figure 6. The patterns at $G/D = 0$ and 0.16 are broadly similar, while at $G/D = 0.031$, the magnitude of the spectral peak is substantially attenuated in the very near region of the wake and the extremum of the contour pattern is displaced a substantial distance downstream. For $G/D = 0.062$, the contours near the slot exit, which represent the undulating jet, are at the lower frequency $f_{o1}/f_o = 0.2$, while those further downstream are at the slightly elevated frequency of large-scale vortex formation $f_{o2}/f_o = 1.2$. These amplitude levels are, however, drastically lower than those at $G/D = 0.031$. For the largest gap of $G/D = 0.125$, the entire near-wake region involves only low-frequency undulations, $f_{o1}/f_o = 0.16$, for the jet undulation, and $f_{o2}/f_o = 1.5$, at a highly attenuated amplitude, in the downstream region of the wake. In other words, there is no indication of classical large-scale vortex formation in the near-wake region.

Figure 7 shows the time-averaged velocity vectors $\langle \boldsymbol{V} \rangle$ at both the midplane and the bed. Consider first the flow patterns at the midplane, $h_L/h_w = 0.5$, given in the left column of images. Generally speaking, for flow past the plain (no slot) cylinder, as well as the cylinder with the smallest slot size $G/D = 0.016$, there exists a well-defined, triangular (dark) strip of low velocity that serves as a demarcation between the downstream-oriented flow and upstream-oriented flow towards the base of the cylinder. At larger slot sizes, $G/D = 0.031$ and 0.062, this triangular demarcation is displaced downstream. In all cases, it terminates in a region of very low velocity magnitude. Correspondingly, at $G/D = 0.031$, the influence of the jet from the slot on the flow in the base region becomes apparent, as it induces two small recirculation cells. At $G/D = 0.062$, the centres of these small-scale cells are displaced downstream. Finally, considering the largest value of gap, $G/D = 0.125$, the relatively large-scale jet dominates, the boundaries of the aforementioned triangular demarcation are no longer evident, and a relatively large region of very low, nearly zero, velocity is evident.

The right column of figure 7 shows the patterns of $\langle \boldsymbol{V} \rangle$ immediately adjacent to the bed, $h_L/h_w = 0.04$. Certain features and trends are broadly similar to those at the midplane indicated in the left column of figure 7, but generally speaking, the patterns become more complex. At $G/D = 0.062$, for example, a substantial number of pockets of very low velocity magnitude are evident, relative to the small number of pockets appearing at the midplane. From figure 7, it is possible to deduce the magnitude of the

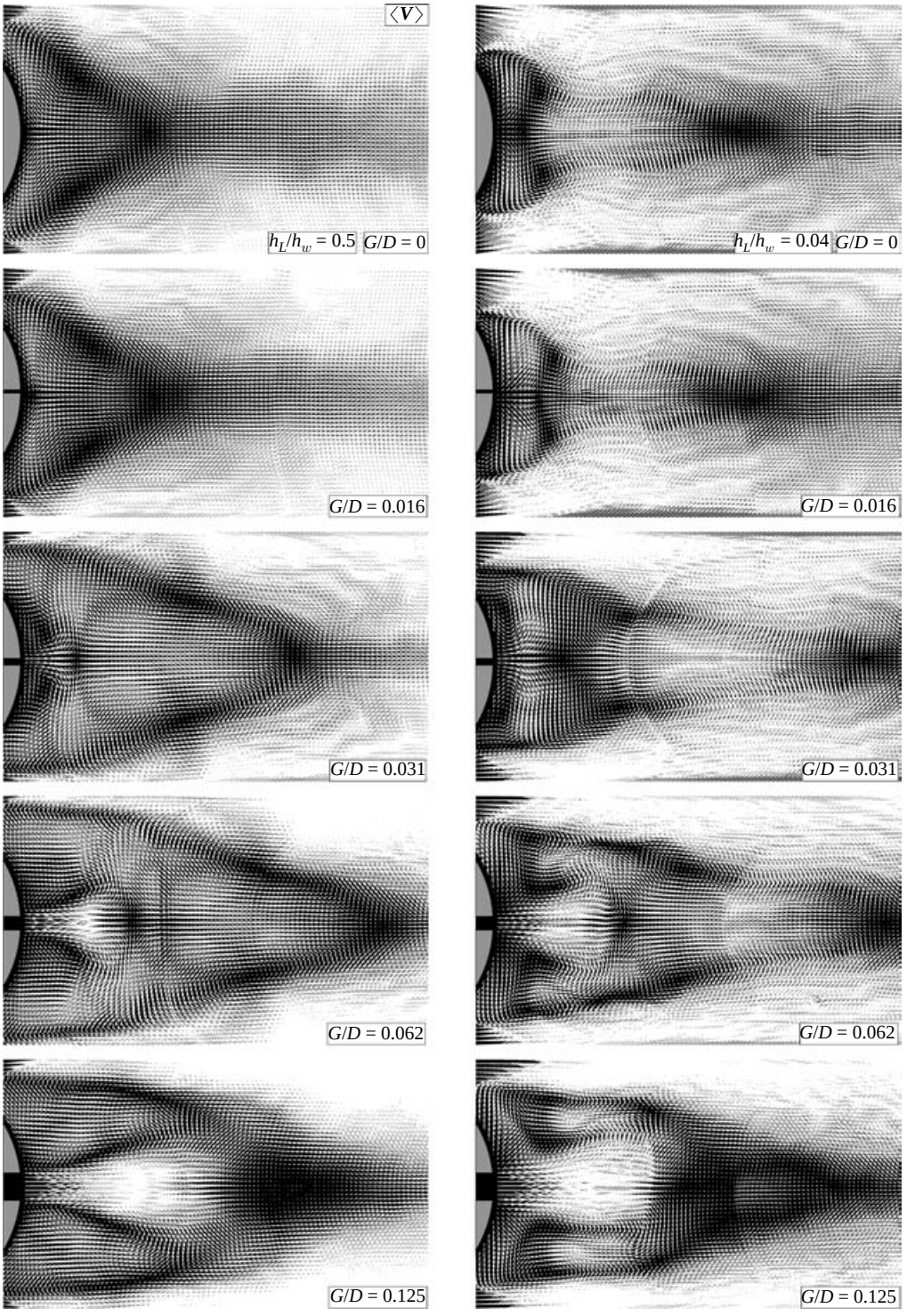

FIGURE 7. Patterns of time-averaged velocity vectors $\langle \boldsymbol{V} \rangle$ at the midplane and immediately adjacent to the bed, $h_L/h_w = 0.5$ and 0.04, for various values of gap width G/D.

reverse flow velocity $\langle u_r \rangle$ along the centreline of the wake. For images at the midplane, $h_L/h_w = 0.5$, and for values of $G/D = 0.031$, 0.062 and 0.125, the maximum upstream-oriented velocity $\langle u_r \rangle_{\max}$, normalized by the free-stream velocity U, has values of $\langle u_r \rangle_{\max}/U = -0.30$, -0.25 and -0.09, at the respective locations $x/D = 1.23$, 1.50 and 1.60, measured from the centre of the cylinder. These magnitudes of reverse velocity correspond to $R = (\langle u_r \rangle_{\max} - U)/(\langle u_r \rangle_{\max} + U) = -1.86$, -1.67 and -1.20 (Monkewitz 1988; Chen & Jirka 1997). In their experimental investigation of shallow wakes from a plain (non-porous) cylinder, Chen & Jirka (1995) found that the maximum return velocity is constant at $\langle u_r \rangle_{\max}/U = -0.35$ ($R = -2.07$) in the unsteady bubble and vortex shedding regimes, for values of the stability parameter $S < 0.5$. Chen & Jirka (1997) analytically consider the onset of absolute versus convective instabilities in the near wake as a function of $\langle u_r \rangle_{\max}/U$, R and S. A direct comparison with the present investigation is not appropriate, since the experiments herein involve a localized jet in the near-wake region, which distorts the form of the velocity profile, relative to a non-locally disturbed profile from a plain cylinder.

All of the features of the time-averaged patterns of velocity $\langle \boldsymbol{V} \rangle$ given in figure 7 are most effectively interpreted in conjunction with the corresponding patterns of time-averaged streamlines $\langle s \rangle$ given in figure 8. In the left column, patterns corresponding to the topology at the midplane, $h_L/h_w = 0.5$, are shown for increasing values of G/D. At $G/D = 0$, as well as 0.016, the form of the topology is relatively simple. It involves a saddle point S_1, as well as a focus F_a and its counterpart on the lower side of the wake. For a larger value of $G/D = 0.031$, where substantial attenuation of the large-scale vortex formation was evident in previous figures, the form of the topology becomes somewhat more complex. An additional saddle point S_2 occurs along the plane of symmetry and, furthermore, a well-defined recirculation cell represented by focus F_b, as well as its counterpart on the opposite side of the wake, are clearly apparent. At $G/D = 0.062$, these critical points retain their identity, but all are displaced significantly in the downstream direction. At the largest value of $G/D = 0.125$, saddle point S_1 is no longer identifiable within the field of view, saddle S_2 has moved downstream a large distance, and a new saddle S_a and its mirror image counterpart have appeared. Furthermore, a new focus F_c and its mirror image are evident.

The corresponding patterns of topology immediately adjacent to the bed are shown in the right column of figure 8. This topology shows, at $G/D = 0$ and 0.016, a saddle point S_2 on the plane of symmetry, as well as an additional saddle point S_a and its mirror image counterpart. The pattern of critical points, involving saddle points S_1 and S_2, along with the focus F_a and its mirror image counterpart, constitute a topology known as an owl face of the first kind, which has been characterized in the area of aerodynamics by Perry & Chong (1986). For $G/D = 0.031$, where, according to previous figures, the large-scale vortex formation has been displaced downstream a substantial distance, the critical points S_1, S_2, F_a, and S_a have all moved downstream significantly and, in addition, new foci F_b and F_c, along with their mirror image counterparts, are now identifiable. At $G/D = 0.062$, a substantial transformation of the pattern occurs. Nevertheless, the basic critical points defined in the foregoing image are identifiable, along with a new saddle point S_b. Finally, at $G/D = 0.125$, the topological pattern degenerates to the form indicated, whereby only the saddle points S_1, S_a and the focus F_c are identifiable.

The patterns of time-averaged velocity $\langle \boldsymbol{V} \rangle$ and streamline $\langle s \rangle$ topology indicated in the foregoing are associated with alterations of Reynolds stresses in the near-wake region. The images of figure 9 show contours of constant Reynolds stress $\langle u'v' \rangle/U^2$ at

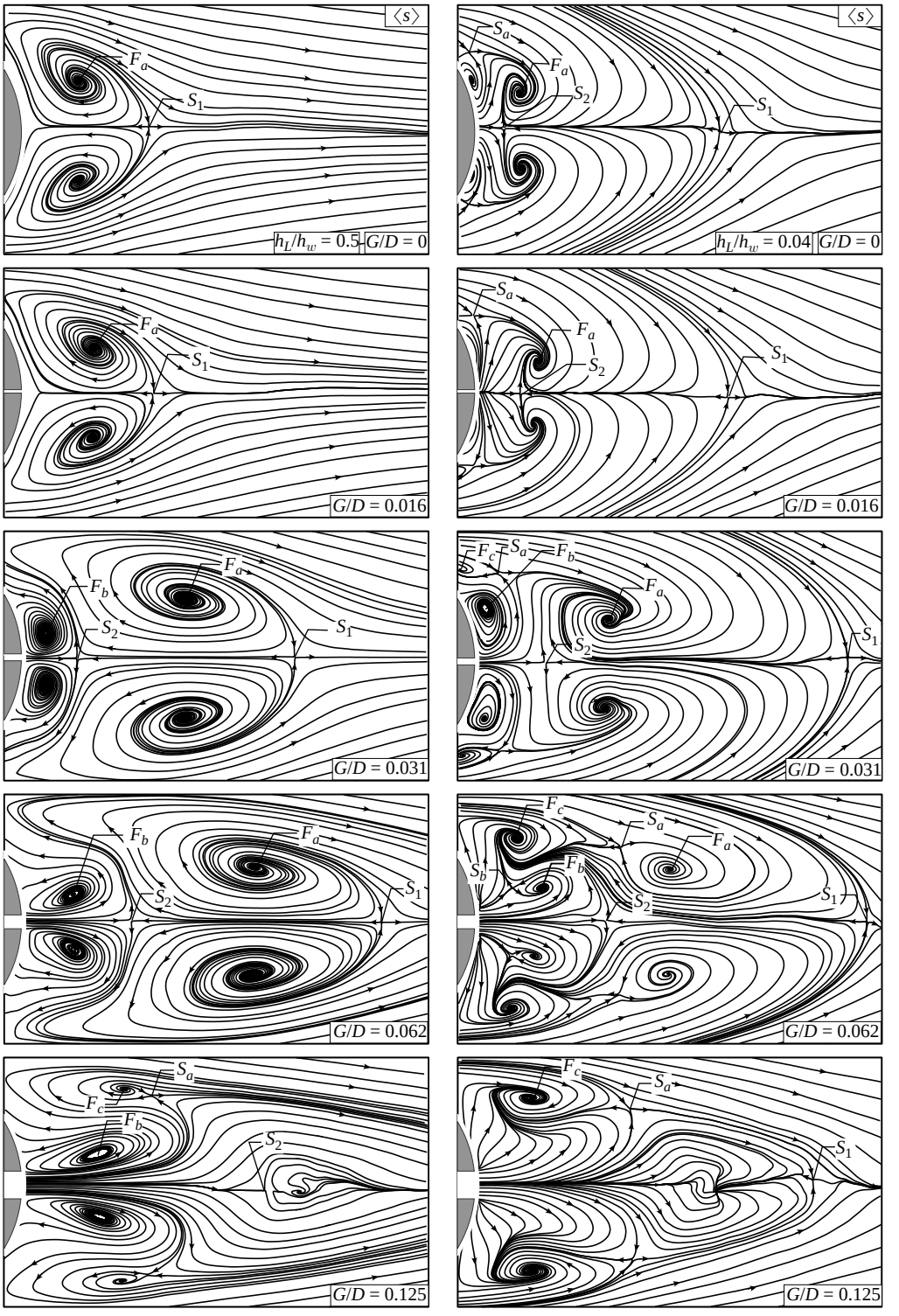

FIGURE 8. Patterns of time-averaged streamline topology $\langle s \rangle$ at the midplane and immediately adjacent to the bed for various values of gap width G/D.

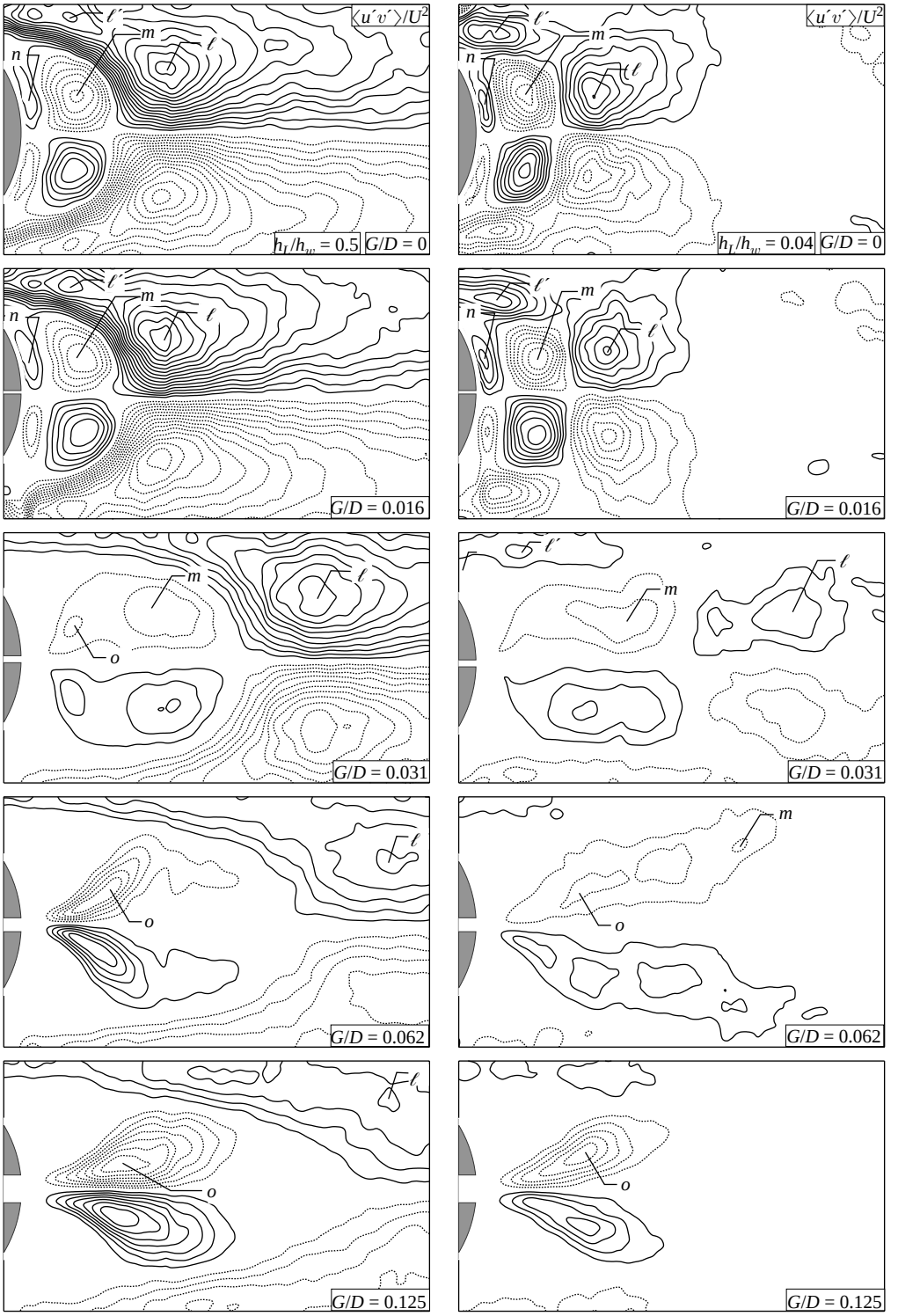

FIGURE 9. Patterns of Reynolds stress correlation $\langle u'v' \rangle / U^2$ at the midplane and immediately adjacent to the bed, $h_L/h_w = 0.5$ and 0.04, for various values of gap width G/D. Minimum and incremental values of Reynolds stress are $[\langle u'v' \rangle / U^2]_{\min} = \pm 0.01$ and $\Delta[\langle u'v'/U^2] = 0.01$. Dotted lines show negative values.

the midplane $h_L/h_w = 0.5$, and at the bed, $h_L/h_w = 0.04$. For the images shown in the left column, representing the midplane elevation, the pattern of $\langle u'v' \rangle / U^2$ shows well-defined clusters ℓ and m, which are characteristic of a near wake of large spanwise extent with large-scale Kármán-like vortex formation, as calculated numerically, for example, by Balachandar, Mittal & Najjar (1997). In addition, identifiable clusters ℓ' associated with the separating shear layer, and n linked to the induced vorticity layer along the surface of the cylinder, are also evident. At the smallest gap width $G/D = 0.16$, these clusters of $\langle u'v' \rangle / U^2$ have a generally similar form to that at $G/D = 0$. When the gap reaches a threshold value of $G/D = 0.031$, however, the peak values of $\langle u'v' \rangle / U^2$ are significantly attenuated and move a substantial distance downstream. In addition, an extremum o is also evident. For the largest values of $G/D = 0.62$ and 0.125, only the peak values ℓ and o are evident.

Immediately adjacent to the bed, as shown in the right column of figure 9, the same extrema ℓ, m, ℓ' and n are identifiable. They occur at approximately the same spatial locations as at the midplane elevation. The details of these patterns do, however, show differences relative to those at the midplane. At $G/D = 0.031$, the locations of the extrema ℓ and m have moved downstream substantially, while experiencing considerable attenuation. At $G/D = 0.062$, the pattern of $\langle u'v' \rangle / U^2$ is distorted in the form indicated, and at $G/D = 0.125$, shows a well-defined extremum o. Regarding magnitudes of the Reynolds stresses at the bed, it is evident that when a threshold value of gap $G/D = 0.031$ is attained, the magnitudes of $\langle u'v' \rangle / U^2$ show a marked decrease. From the foregoing figures, this case corresponds to a substantial retardation of the onset of large-scale vortex formation in the near wake. Moreover, it is apparent that the unsteadiness associated with the developing jet from the slot does not locally enhance the Reynolds stresses in this region. On the other hand, it is evident that when the gap becomes sufficiently large, $G/D = 0.125$, for which the corresponding momentum of the jet has a significantly large value, locally large values of $\langle u'v' \rangle / U^2$ are attainable in the region of jet formation.

6. Near-wake structure due to combined base bleed and rotational perturbations

It is apparent from the aforementioned sections that base bleed through a slot can substantially retard the onset and development of large-scale vortical structures in the near-wake region, relative to those occurring from a plain cylinder. The issue arises as to whether it is possible to recover large-scale vortices in the presence of slot bleed, by appropriate rotational perturbations of the cylinder.

Figure 10 shows phase-averaged patterns of the flow structure. The phase reference corresponds to the same instantaneous angular position ($\theta = -14^\circ$) during the oscillation cycle of the cylinder, which is perturbed at the inherent frequency of large-scale vortex formation; the amplitude of the perturbation is $A/D = 0.2(\theta_{Max} = \pm 23^\circ)$. The patterns of phase-averaged velocity $\boldsymbol{V}_p$ and streamlines s_p show that, for the case of the plain ($G/D = 0$) cylinder, the initially formed, large-scale vortex is from the upper side of the cylinder, whereas for the case of $G/D = 0.031$, it is from the lower surface of the cylinder. This point is further emphasized by inspection of the vorticity contours $\langle \omega \rangle_p$ shown in the right column. The insets in each of these images of $\langle \omega \rangle_p$ show the time-dependence of the tangential velocity v_e of the cylinder, and the vertical velocity component v_Q at the reference location Q indicated in the patterns of $\langle s \rangle_p$. These plots further verify the switch in phase of the initially formed vortex. It

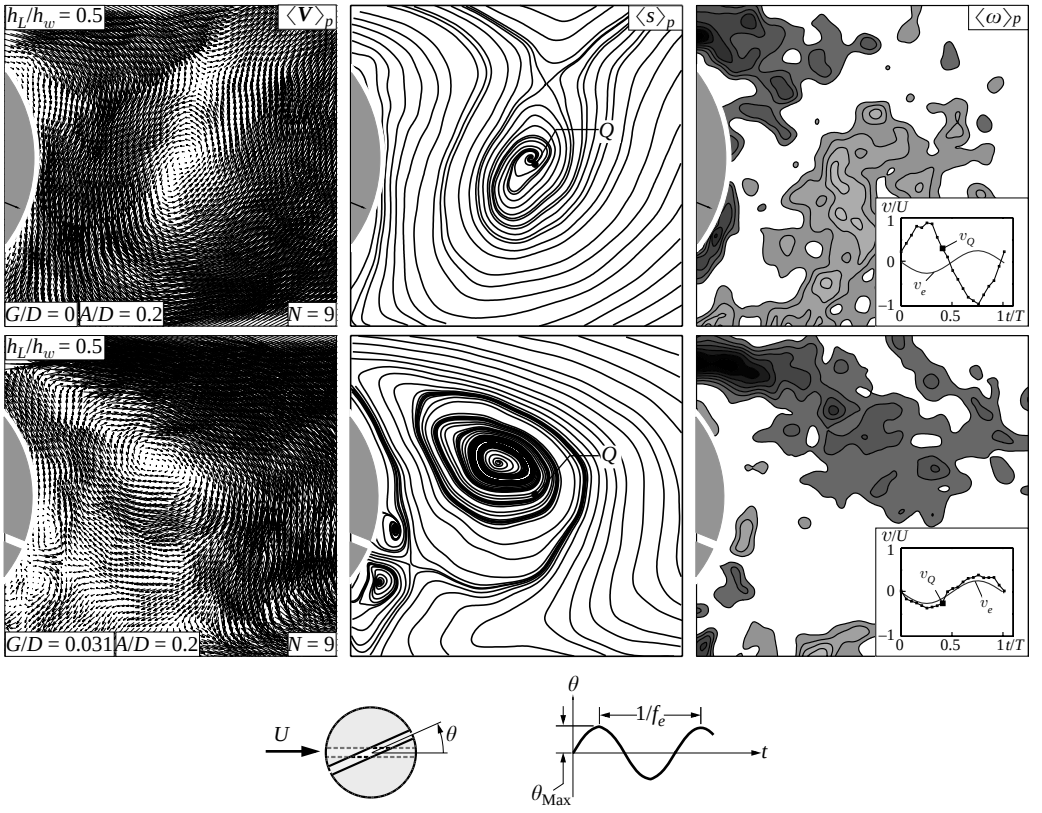

FIGURE 10. Phase-averaged flow patterns at the same phase of the rotational motion of cylinder for an amplitude of $A/D = 0.2$. Phase-averaged velocity $\langle \boldsymbol{V} \rangle_p$, streamline topology $\langle s \rangle_p$ and vorticity contours $\langle \omega \rangle_p$ are shown on midplane for near wakes of the plain cylinder and slotted cylinder. In the inset of the $\langle \omega \rangle_p$ images, the tangential velocity v_e of the cylinder is plotted along with the time history of the vertical velocity v_Q at location Q in the near wake.

is therefore evident that a small-magnitude base bleed can have a large effect on the timing of the initially formed vortex relative to the cylinder motion. This aspect has important consequences for the direction of energy transfer between the fluid and the oscillating cylinder.

Corresponding time-averaged patterns of the wake structure are given in figure 11. The top two rows of images compare cases of no slot and a relatively narrow slot, $G/D = 0$ and 0.31, for the case of the stationary cylinder. The third row of images shows the consequence of applied perturbations at the inherent frequency of large-scale vortex formation from the plain cylinder, but in the presence of the gap $G/D = 0.031$. The recirculation cells immediately adjacent to the base of the cylinder, as well as the saddle point adjacent to these cells, evident in the middle image for $G/D = 0.031$ and $A/D = 0$, are eliminated in the bottom $\langle s \rangle$ image for excitation at $A/D = 0.2$. Moreover, a saddle point now appears downstream of the large-scale spiral streamline pattern near the right side of the image. The overall form of the pattern of streamline topology, as well as the associated pattern of averaged velocity $\langle \boldsymbol{V} \rangle$, are generally similar to those of the plain cylinder without a slot, i.e. $G/D = 0$ shown in the first row of images. Furthermore, as shown in the right column of images, it is evident that such rotational perturbations tend to transform the patterns

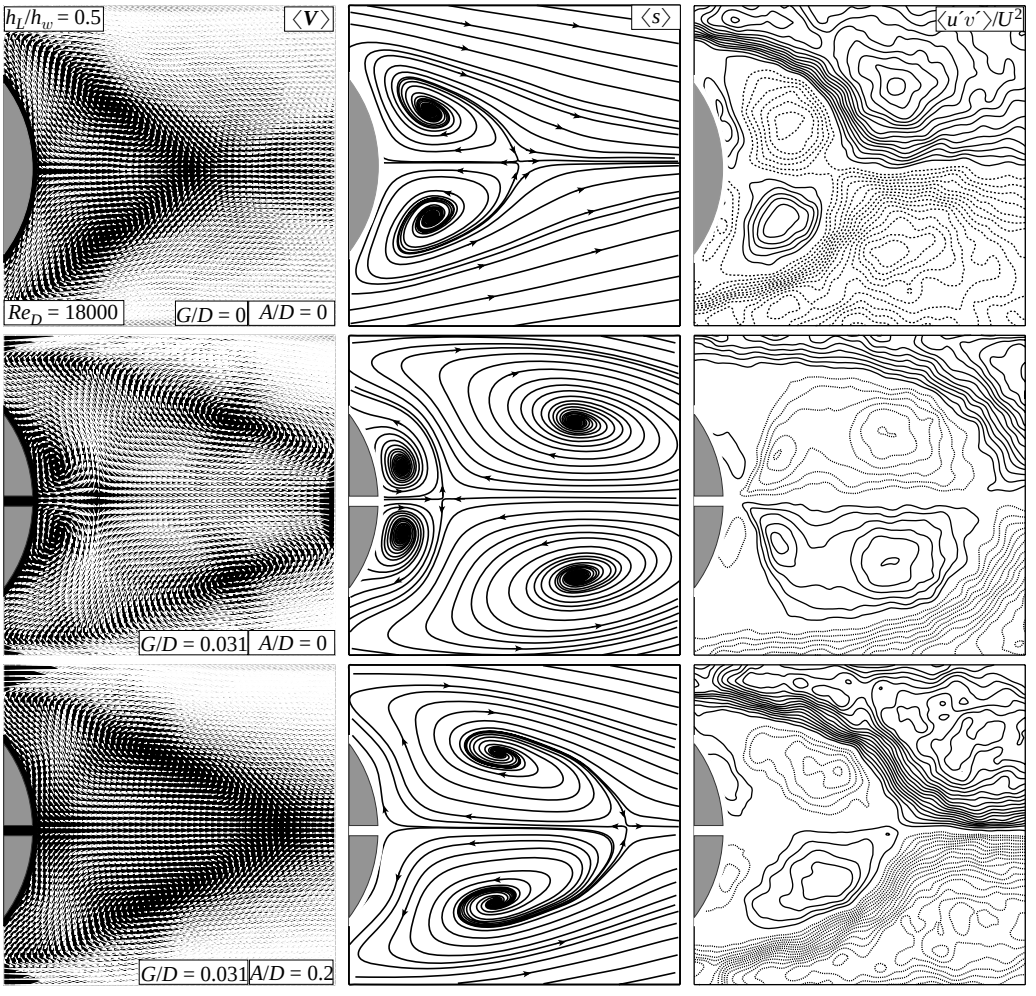

FIGURE 11. Time-averaged patterns of the wake of a slotted cylinder with gap width $G/D = 0.031$, with and without perturbation at an amplitude of $A/D = 0.2$, in comparison with patterns from a stationary plain cylinder.

of Reynolds stress correlation $\langle u'v' \rangle / U^2$ to a form generally similar to those from the plain stationary cylinder ($G/D = 0$) indicated in the first row of images. In fact, this pattern of $\langle u'v' \rangle / U^2$ is quite different from that shown in the middle image of the right column of figure 11, corresponding to the case of slot bleed $G/D = 0.031$ in the absence of rotational perturbation.

7. Concluding remarks

Shallow flow past a cylinder gives rise to a horseshoe (necklace) vortex system about the upstream surface of the cylinder, and large-scale vortex formation in the near wake. Furthermore, the existence of a negative base pressure on the downstream surface of the cylinder, in conjunction with time-averaged patterns of recirculation cells, are also well-known inherent features of the very near wake. The consequence of a streamwise slot through the cylinder is to alter the patterns of the flow structure

along the fore and base regions of the cylinder, as well as in its near wake. Such alterations have important implications, not only for the steady and unsteady loading on the cylinder, but also the corresponding loading on the bed region about the cylinder.

The horseshoe vortex that exists about the upstream surface of the cylinder without a slot can be altered significantly via flow extraction through a slot. Such extraction substantially decreases the vertical gradient of circumferential vorticity along the plane of symmetry, in accordance with loss of the well-defined cluster of vorticity that represents the horseshoe vortex. Furthermore, the streamline topology along the bed, in particular the number and location of critical points, is fundamentally transformed.

In the near-wake region, the process of large-scale vortex formation is substantially retarded, i.e. the centre of the first fully formed vortex moves downstream, when a threshold value of gap width G/D is attained. It corresponds to a very low value of the momentum coefficient c_μ of the jet from the slot. At this threshold, a jet-like flow of very low magnitude issues from the exit of the slot at the cylinder base, and undergoes transverse undulations. If the slot size G/D is sufficiently large, the dimensionless frequency of the undulations is nearly an order of magnitude smaller than the formation frequency of large-scale vortices.

The foregoing physics of the near wake can be interpreted in terms of patterns of time-averaged vorticity, as well as contours of constant spectral amplitude, both evaluated over entire planes at and above the bed. These patterns are dramatically distorted in the downstream direction at the threshold values of G/D and c_μ, relative to the case of the cylinder without bleed.

Furthermore, the consequences of bleed flow through the slot for the structure of the near wake can be categorized via critical points, i.e. saddle points and foci. Such patterns take on increasingly complex forms at successively larger values of bleed, especially in the region immediately adjacent to the bed. The increased complexity of the bed topology is associated with reduced magnitudes of the dimensionless Reynolds stress correlations at the threshold values of G/D and c_μ, relative to the case of no bleed. This observation suggests significant reductions in bed loading, over the entire near wake region, for relatively small values of base bleed.

When the formation process of large-scale vortices in the very near wake is substantially attenuated, or retarded, via small bleed at the aforementioned threshold values of G/D and c_μ, rotational perturbation of the cylinder can lead to patterns of streamline topology and contours of Reynolds stress correlation that have an overall form similar to the patterns associated with the plain (no slot) cylinder in the absence of perturbation. That is, recovery of the form of the naturally occurring wake structure is attainable. A further consequence of cylinder perturbation, in the presence of base bleed of very small magnitude, is to induce a value of phase shift, or timing, of the initially formed vortex that is fundamentally different from the phase shift associated with perturbations of the plain cylinder.

The authors are pleased to acknowledge financial support of the National Science Foundation through Grant CTS-0228110, as well as supplemental support through the Office of Naval Research Grant N00014-94-1-0185 and the Air Force Office of Scientific Research, Grant F49620-02-1-0061.

REFERENCES

Akilli, H. & Rockwell, D. 2002 Vortex formation from a cylinder in shallow water. *Phys. Fluids* **14**, 2957–2967.

Balachandar, S., Mittal, R. & Najjar, F. M. 1997 Properties of the mean wake recirculation region in two-dimensional bluff body wakes. *J. Fluid Mech.* **351**, 167–199.

Balachandar, R., Ramachandran, S. & Tachie, M. F. 2000 Characteristics of shallow turbulent near wakes at low Reynolds numbers. *Trans. ASME: J. Fluids Engng* **122**, 302–308.

Balachandar, R., Tachie, M. F. & Chu, V. H. 1999 Concentration profiles in shallow turbulent wakes. *Trans. ASME: J. Fluids Engng* **121**, 34–43.

Bearman, P. W. 1967 The effect of base bleed on the flow behind a two-dimensional model with a blunt trailing-edge. *Aero. Quart.* **18**, 207–225.

Carmer, C. F. V., Rummel, A. & Jirka, G. H. 2002 Combined planar measurements of flow velocity and mass concentration in shallow turbulent flow. Part 2: Application of coupled PIV-PCA technique to turbulent shallow wake flows. *Proc. ASCE/IAHR Intl Conf. on Hydraulic Measurements and Experimental Methods, Estes Park, USA.*

Carmer, C. F. V., Rummel, A. C. & Jirka, G. H. 2003 Influence of secondary motion in large-scale coherent vortical structures on the mass transport in a shallow turbulent wake flow. *Proc. Intl Symp. Shallow Flows, Technical University of Delft, Netherlands, June 16–18* (ed. G. H. Jirka & W. S. J. Uijttewall), Part 3, pp. 129–136. See also *Shallow Flows* (ed. G. H. Jirka & W. S. J. Uijttewall), pp. 103–110. A. A. Balkema.

Carmer, C. F. V., Weitbrecht, V. & Jirka, G. H. 2001 On the genesis and fate of large coherent vortical structures in turbulent shallow wake flows. *Proc. 2001 Intl Symp. on Environmental Hydraulics.*

Castro, I. P. 1971 Characteristics of two-dimensional perforated plates normal to an air-stream. *J. Fluid Mech.* **46**, 599–609.

Chen, D. & Jirka, G. H. 1995 Experimental study of plane turbulent wakes in a shallow water layer. *Fluid Dyn. Res.* **16**, 11–41.

Chen, D. & Jirka, G. H. 1997 Absolute and convective instabilities of plane turbulent wakes in a shallow water layer. *J. Fluid Mech.* **338**, 157–172.

Devenport, W. J. & Simpson, R. L. 1990 Time-dependent and time-averaged turbulence structure near the nose of awing-body junction. *J. Fluid Mech.* **210**, 23–55.

Grubisic, V., Smith, R. B. & Schar, C. 1995 The effect of bottom friction on shallow-flow past an isolated obstacle. *J. Atmos. Sci.* **48**, 1985–2006.

Huerre, P. & Monkewitz, P. A. 1990 Local and global instabilities in spatially developing flows. *Annu. Rev. Fluid Mech.* **22**, 473–539.

Igarashi, T. 1978 Flow characteristics around a circular cylinder with a slit. *Bull. Japan. Soc. Mech. Engrs* **21**, 656–664.

Ingram, G. R. & Chu, V. H. 1987 Flow around islands in Rupert bay: an investigation of the bottom friction effect. *J. Geophys. Res.* **92** (C13), 14521–14533.

Inoue, O. 1985 A new approach to flow problems past a porous plate. *AIAA J.* **23**, 1916–1921.

Kahraman, A., Sahin, B. & Rockwell, D. 2002 Control of vortex formation from a vertical cylinder in shallow water: Effect of localized roughness. *Exps. Fluids* **33**, 54–65.

Kirgöz, S. & Ardiclioglue, M. 1997 Velocity profiles of developing and developed open channel flow. *J. Hydraul. Engng* **123**, 1099–1105.

Lawless, M. R., Lane, S. N. & Best, J. L. 2003 The junction vortex system: time-mean and instantaneous flow fields *Proc. Intl Symp. Shallow Flows, Technical University of Delft, Netherlands, June 16–18*, Part 3, pp. 137–144.

Lloyd, P. M. & Stansby, P. K. 1997 Shallow water flow around model conical islands of small side slope. *J. Hydraulic Engng* **123**, 1057–1067.

Lloyd, P. M., Stansby, P. K. & Chen, D. 2001 Wake formation around islands in oscillatory laminar shallow-water flows. Part 1. Experimental investigation. *J. Fluid Mech.* **429**, 217–238.

Monkewitz, P. A. 1998 The absolute and convective nature of instability in two-dimensional wakes at low Reynolds numbers. *Phys. Fluids* **31**, 999–1006.

Newland, D. E. 1993 *An Introduction to Random Vibrations, Spectral & Wavelet Analysis*, third Edn. pp. 113–124, Longman.

Perry, A. E. & Chong, M. S. 1986 A series-expansion study of the Navier-Stokes equations with applications to three-dimensional separation patterns. *J. Fluid Mech.* **173**, 207–223.

Perry, A. E. & Steiner, T. R. 1987 Large-scale vortex structures in turbulent wakes behind bluff bodies. Part 1. Vortex formation. *J. Fluid Mech.* **174**, 233–270.

Praisner, T. J., Sabatino, D. R. & Smith, C. R. 2001 Simultaneously combined liquid-crystal surface heat transfer and PIV flow-field measurements. *Exps. Fluids* **30**, 1–10.

Praisner, T. J., Seal, C., Takmaz, L. & Smith, C. R. 1997 Spatial-temporal flow-field and heat transfer behavior in end-wall junctions. *Intl J. Heat Fluid Flow* **18**, 142–151.

Schar, C. & Smith, R. B. 1993 Shallow-water flow past isolated topography. Part II: Transition to vortex shedding. *J. Atmos. Sci.* **40**, 1401–1412.

Seal, C. V. & Smith, C. R. 1999 Visualization of a mechanism for three-dimensional interaction and near-wall eruption. *J. Fluid Mech.* **394**, 193–203.

Seal, C., Smith, C. R. & Rockwell, D. 1997 Dynamics of the vorticity distribution in end-wall junctions. *AIAA J.* **35**, 1041–1047.

Simpson, R. L. 2001 Juncture flows. *Annu. Rev. Fluid Mech.* **33**, 415–443.

Smith, R. B. & Grubisic, V. 1993 Aerial observations of Hawaii's wake. *J. Atmos. Sci.* **50**, 3728–3750.

Tachie, M. F. & Balachandar, R. 2001 Shallow wakes generated on smooth and rough surfaces. *Exps. Fluids* **30**, 467–474.

Visbal, M. R. 1991 Structure of laminar juncture flows. *AIAA J.* **29**, 1273–1282.

Visbal, M. R. & Gordnier, R. E. 1994 Crossflow topology of vortical flows. *AIAA J.* **32**, 1085–1087.

Wong, H. Y. 1985 Wake stabilization by the action of base bleed. *Trans. ASME: J. Fluids Engng* **107**, 378–384.

Wood, C. J. 1964 The effect of base bleed on a periodic wake. *J. R. Aero. Soc.* **68**, 477–482.

Wood, C. J. 1967 Visualization of an incompressible wake with base bleed. *J. Fluid Mech.* **29**, 259–272.

Zhong, J., Huang, T. S. & Adrian, R. J. 1998 Extracting 3D Vortices in Turbulent Fluid Flow. *IEEE Trans. Pattern Anal. Machine Intell.* **20**, 193–199.